International Journal of Nanomedicine

Dovepress
open access to scientific and medical research

Open Access Full Text Article

ORIGINAL RESEARCH

Polyaniline-coated upconversion nanoparticles with upconverting luminescent and photothermal conversion properties for photothermal cancer therapy

This article was published in the following Dove Press journal:
International Journal of Nanomedicine
2 September 2016
Number of times this article has been viewed

Yadong Xing
Luoyuan Li
Xicheng Ai
Limin Fu

Department of Chemistry, Renmin University of China, Beijing, People's Republic of China

Abstract: In this study, we developed a nanosystem based on upconversion nanoparticles (UCNPs) coated with a layer of polyaniline nanoparticles (PANPs). The UCNP induces upconversion luminescence for imaging and photothermal conversion properties are due to PANPs. In vitro experiments showed that the UCNPs-PANPs were nontoxic to cells even at a high concentration (800 μg mL^{-1}). Blood analysis and histological experiments demonstrated that the UCNPs-PANPs exhibited no apparent toxicity in mice in vivo. Besides their efficacy in photothermal cancer cell ablation, the UCNP-PANP nanosystem was found to achieve an effective in vivo tumor ablation effect after irradiation using an 808 nm laser. These results demonstrate the potential of the hybrid nanocomposites for use in imaging-guided photothermal therapy.

Keywords: upconversion nanoparticles, polyaniline, upconversion luminescence, photothermal therapy

Introduction

Photothermal therapy (PTT) is based on controlling the conversion of light into heat, which can employed to ablate diseased (ie, cancerous) tissues.[1] During PTT treatment, heat is generated by the interaction between laser light and PTT coupling agents, and the heat can be localized to areas where the PTT coupling agents and the applied light overlap. Therefore, compared with traditional cancer therapies, such as surgery, radiotherapy, and chemotherapy, PTT allows excellent spatial control and prevents excessive off-target damage. Currently, the available PTT coupling agents mainly consist of metal nanoparticles (Au, Ag, Pd, Ge, etc),[2–9] semiconductor nanoparticles (CuS, CuSe, etc),[9–12] carbon-based nanomaterials (carbon nanotubes, graphenes, etc),[13] and polymeric nanoparticles (polyaniline, polypyrrole, poly[3,4-ethylenedioxythiophene], etc).[14–28] Polymeric nanoparticles have been widely explored by several different groups for use in PTT to treat cancer. Among the most popular polymeric nanoparticles, polyaniline is the oldest and potentially one of the most useful conducting polymers due to its conductivity, mechanical flexibility, low cost, and noncytotoxicity. Previously, polyaniline nanoparticles (PANPs) have been successfully used as photothermal coupling materials for PTT both in vitro and in vivo due to their excellent photostability, biodegradability, good biocompatibility, and high photothermal conversion efficiency.[29,30] However, to facilitate more precise therapy, further research is still needed to develop diagnostic and imaging components in a single nanosystem.

Correspondence: Yadong Xing; Limin Fu
Department of Chemistry, Renmin University of China, No 59 Zhongguancun Street, Beijing 100872, People's Republic of China
Tel +86 10 6251 6604
Fax +86 10 6251 6444
Email xingyadong@ruc.edu.cn; lmfu@chem.ruc.edu.cn

submit your manuscript | www.dovepress.com
Dovepress
http://dx.doi.org/10.2147/IJN.S97441

In addition, due to the availability of lanthanide elements with unique 4*f* electron structures, the doping of lanthanide ions (a sensitizer of Yb^{3+} and an activator of Er^{3+}/Tm^{3+}/Ho^{3+}, etc) in nanoparticles can yield a unique upconversion luminescence (UCL) process, where low-energy light is converted into high-energy light via sequential multiple photon absorptions or energy transfers.[31] Thus, lanthanide-based upconversion nanoparticles (UCNPs) have special optical characteristics, such as sharp emission lines, large anti-Stokes shifts of several hundred nanometers, and the absence of autofluorescence in biosamples.[32–38] Therefore, UCNPs have been recently used as building blocks in the construction of multimodal contrast agents for imaging-guided therapy.[39–45]

In the current study, upconversion nanoparticles (UCNPs) were first prepared by a typical solvothermal method. A polyaniline photothermal therapeutic shell was then formed by the polymerization of an aniline monomer in acid aqueous conditions, thereby obtaining polyaniline-coated UCNPs (UCNPs-PANPs). The UCL properties, photothermal conversion efficiency, and safety of the developed UCNPs-PANPs were assessed. In addition, their potential use in cancer treatment with mice bearing tumors was evaluated to determine their PTT efficacy.

Materials and methods

Materials

Rare-earth oxides Lu_2O_3 (99.99%), Yb_2O_3 (99.9%), and Er_2O_3 (99.9%) were purchased from Beijing Lansu Co. (Beijing, People's Republic of China). Oleic acid (OA, 90%) was purchased from Sigma-Aldrich Co. (St Louis, MO, USA). 1-Octadecene (ODE, 90%), ammonium fluoride (NH_4F, 98%), and tetrafluoroborate ($NOBF_4$) were purchased from Alfa Aesar Ltd. Aniline was purchased from Tianjin Guangfu Technology Development Co. Ltd. Ethanol, cyclohexane, dichloromethane (CH_2Cl_2), sodium dodecyl benzene sulfonate, and polyvinyl alcohol were purchased from Sinopharm Chemical Reagent Co., Ltd. (Beijing, People's Republic of China). Ammonium persulfate ($(NH_4)_2S_2O_8$), sodium hydroxide (NaOH), and hydrochloric acid (HCl) were purchased from Beijing Chemical Works. Deionized water was used throughout. Rare-earth chlorides ($LnCl_3$, Ln: Lu, Yb, Er) were prepared by dissolving the corresponding metal oxide in 10% HCl at elevated temperature and then evaporating the water completely under reduced pressure. All the chemicals used were of analytical grade and were used without further purification.

Synthesis of UCNPs-PANPs

Synthesis of OA-coated UCNPs

OA-coated UCNPs were synthesized according to a previous method.[46] Next, 6 mL OA and 15 mL ODE were added into a 100 mL three-necked flask containing $LuCl_3$ (0.78 mmol), $YbCl_3$ (0.20 mmol), and $ErCl_3$ (0.02 mmol). The mixture was heated to 160°C at argon atmosphere to form a homogeneous and transparent solution and then cooled down to room temperature. NaOH (2.5 mmol) and NH_4F (4 mmol) were incorporated into the flask and stirred for 30 minutes. Subsequently, the solution was heated to 295°C and maintained for 1 hour at argon atmosphere. After the solution was cooled naturally, an excess amount of ethanol was poured into the resultant mixture and centrifugally separated, and the products were collected and washed with ethanol three times.

Synthesis of UCNPs-PANPs

The bald UCNPs were obtained from the OA-coated UCNPs through a ligand-free process.[47] OA-coated UCNPs (10 mg) were added into a flask containing certain amount of oversaturated $NOBF_4$ solution. The mixture was dispersed under sonication for 10 minutes and then was centrifugally separated.

The UCNPs-PANPs were synthesized by an in situ chemical oxidative polymerization. In a typical procedure, 10 mg bald UCNPs were added into an aqueous solution containing 5 mg sodium dodecyl benzene sulfonate and 15 mg polyvinyl alcohol. The solution was then ultrasonicated to make well-dispersed bald UCNPs. Then, the solution was stirred at room temperature for 30 minutes and 5 μL of aniline monomer was added. After further stirring for 30 minutes, 30 mg $(NH_4)_2S_2O_8$ was added into the reaction mixture to induce the polymerization reaction. The mixture was then polymerized for 5 hours at room temperature to obtain UCNPs-PANPs with a dark green color. For bioapplication, UCNPs-PANPs were further capped with F127 according to the previous literature.[30]

Characterization

The sizes and morphologies of UCNPs and UCNPs-PANPs were characterized using a Tecnai G^2F30 transmission electron microscopy (TEM) under 300 kV accelerating. Samples were dispersed in cyclohexane or ethanol and dropped on the surface of a copper grid. Energy-dispersive X-ray (EDX) analysis of the UCNPs was also performed during high-resolution

TEM measurements. Powder X-ray diffraction (XRD) measurement was measured with a Bruker D8 advance X-ray diffractometer from 10° to 90° (Cu Kα radiation, λ=1.54 Å). Ultraviolet–visible–near infrared (UV–vis–NIR) absorption spectra were obtained on a Shimadzu UV-3600 UV–vis–NIR spectrophotometer. The nanoparticles were dispersed in ethanol to measure the UV–vis–NIR spectra. UCL spectra were measured with a Maya2000 Pro fluorescence spectrometer, using an external 0–5 W adjustable continuous wavelength laser at 980 nm, as the excitation source. Zeta potential and hydrodynamic diameter were measured on a Zetasizer nano 90. To ensure the accuracy of size distribution measurement, great care was taken to eliminate dust from the sample. The aqueous solution of the UCNPs-PANPs was filtered through two membrane filters with 0.45 µm nominal pore size connected in series.

Cell culture

A human colon carcinoma cell line (U87MG) was provided by the American Type Culture Collection. The cells were grown in Modified Eagle's Medium (MEM) supplemented with 10% fetal bovine serum at 37°C under 5% CO_2. This study was approved by the ethics committee of Renmin University of China.

Photothermal properties

The photothermal conversion efficiency (η value) of UCNPs-PANPs solution (200 µg mL^{-1}) under 808 nm irradiation (0.8 W cm^{-2}) was calculated using the following equation:[48]

$$\eta = \frac{hA\Delta T_{max} - Q_s}{I\,(1-10^{-A_\lambda})} \quad (1)$$

where h is the heat transfer coefficient, A is the surface area of the container, ΔT_{max} is the temperature change of the UCNPs-PANPs solution at the maximum steady-state temperature, I is the laser power, A_λ is the absorbance of UCNPs-PANPs at a specific wavelength, Q_s is the heat associated with the light absorbance of the solvent, and η is the photothermal conversion efficiency.

The photothermal images of UCNPs-PANPs in solution were obtained using an FLIR E40 equipment running on FLIR tools systems (FLIR Systems, Inc., Wilsonville, OR, USA), in conjunction with an 808 nm laser (Xi'an Sampling Laser Technic Institute). The whole system is set up, including photothermal imaging equipment, laser illuminator (808 nm), laser diode, lens, fibers, and specimen table. Dilutions of UCNPs-PANPs in deionized water (2.0 mg mL^{-1}) were placed in a series of specimen bottles irradiated by an 808 nm laser (0.50 W cm^{-2}, 0.85 W cm^{-2}, and 1.20 W cm^{-2}). The temperature signals recorded at different time intervals (0–120 seconds) were analyzed with FLIR tools systems.

Toxicity of UCNPs-PANPs

Methyl thiazolyl tetrazolium study

In vitro cytotoxicity was measured by performing methyl thiazolyl tetrazolium (MTT) assays on the U87MG cells. Cells (90 µL well^{-1}, 10^5 mL^{-1}) were seeded into 96-well cell culture plate under 100% humidity and were cultured at 37°C and 5% CO_2 for 24 hours; different concentrations of UCNPs-PANPs (0 µg mL^{-1}, 100 µg mL^{-1}, 200 µg mL^{-1}, 400 µg mL^{-1}, 600 µg mL^{-1}, and, 800 µg mL^{-1}, diluted in MEM) were then added to the wells. Six repeated experiments were performed. The cells were subsequently incubated for 4 hours, 24 hours, and 48 hours at 37°C under 5% CO_2.

Thereafter, MTT (10 µL; 5 mg mL^{-1}) was added to each well and the plate was incubated for an additional 4 hours at 37°C under 5% CO_2. After the addition of 10% sodium dodecyl sulfate (100 µL well^{-1}), the assay plate was allowed to stand at room temperature for 12 hours. The optical density OD570 value (absorbance) of each well, with background subtraction at 690 nm, was measured by means of a Tecan Infinite M200 monochromator-based multifunction microplate reader. Equation 2 was used to calculate the inhibition of cell growth:

$$\text{Cell viability (\%)} = \frac{\text{Mean of absorbance value of treatment group}}{\text{Mean Abs. value of control}} \times 100\% \quad (2)$$

Histology and hematology studies

Use of animals in this study was in accordance with the protocol as approved by the Institutional Animal Care and Use Committee (IACUC) according to The NIH Office of Laboratory Animal Welfare (OLAW) guidelines. Blood samples and tissues were harvested from mice (5-week-old) injected intravenously with 100 µL of hydrophilic UCNPs-PANPs (2 mg mL^{-1}) and from mice receiving no injection for comparison at 0.5 hours, 24 hours, 7 days, and 30 days post injection.

Blood was collected from the orbital sinus by quickly removing the eyeball from the socket with a pair of tissue forceps. Five important hepatic indicators (total bilirubin

[TBIL], alanine aminotransferase [ALT], aspartate aminotransferase [AST], total protein [TP], and albumin [ALB]) and one indicator for kidney functions (creatinine [CRE]) were measured. Blood smears were prepared by placing a drop of blood at one end of a slide, and using another slide to disperse the blood along the length of the slide. The slide was left to air-dry, after which the blood was stained with hematoxylin and eosin (H&E). Upon completion of the blood collection, mice were sacrificed. For H&E-stained tissues, main organs of interest (heart, liver, spleen, lung, and kidney) were harvested from mice. The tissues were fixed in 10% formalin, dehydrated with ethanol, embedded in paraffin, sectioned, and stained with H&E. The histological sections were observed under an optical microscope. Three repeated experiments were performed for the histology and hematology studies.

PTT in vitro

Cells were incubated with UCNP-PANP samples (100 μg mL^{-1}) for 4 hours and were washed with phosphate-buffered saline (PBS) three times and resupplied with fresh MEM. After the treatment, the cells were exposed to the 808 nm irradiation (0.5 W cm^{-2}) for 15 minutes. Cells were then stained with propidium iodide (staining dead cells agent) for 10 minutes after washing with PBS solution three times. Fluorescent images were collected at 600−640 nm upon the irradiation of 532 nm.

Tumor xenografts

U87MG cells were harvested when they reached near confluence by incubation with 0.05% trypsin–ethylenediaminetetraacetic acid and were pelleted by centrifugation and resuspended in sterile PBS. Cells (~10^7 cells $site^{-1}$) in 200 μL of MEM were then implanted subcutaneously onto the back of 4-week-old male NU/NU nude mice. Photothermal imaging studies were performed when tumors reached 0.4–0.6 cm in average diameter.

Photothermal imaging in vivo

In vivo photothermal imaging was performed with an FLIR E40 equipment, in conjunction with an 808 nm laser illuminator, which were set up by Zhou et al.[30] NU/NU nude mice bearing tumor were anesthetized (with 10% chloral hydrate, 100 μL), and PBS solution of UCNPs-PANPs (50 μL, 1 mg mL^{-1}) was intratumorally injected into the mouse. After irradiation by the laser of 808 nm (0.5 W cm^{-2}), temperature signals recorded at different time points (0–5 minutes) were analyzed with FLIR tools systems.

PTT in vivo

Test group: PBS solution of UCNPs-PANPs (50 μL, 1 mg mL^{-1}) was intratumorally injected into the mice which were exposed to 808 nm laser (0.5 W cm^{-2}) for 20 minutes (UCNPs-PANPs + laser, n=3). Control groups: mice without the injection of UCNPs-PANPs (laser, n=3) or without 808 nm laser exposure (UCNPs-PANPs, n=3). Blank group: mice with no injection of UCNPs-PANPs and without 808 nm laser exposure (blank, n=3). After the treatment, the tumor sizes were measured by a caliper every day and calculated as volume = (tumor length) × (tumor width)^2/2. Relative tumor volumes were calculated as V/V_0 (V_0 is the tumor volume when the treatment was initiated). The life spans of the mice were tracked until the mice died naturally.

Results

Synthesis and characterization of UCNPs-PANPs

First, OA-coated $NaLuF_4$ nanoparticles doped with Yb^{3+}, Er^{3+} (UCNPs) were synthesized by a solvothermal method using OA as the surface ligand and ODE as a solvent. The OA-coated UCNPs were soluble in nonpolar solvents, such as cyclohexane. The size and morphology of the OA-coated UCNPs were characterized by TEM. As shown in Figure 1, the OA-coated UCNPs were almost spherical in shape and they measured ~34.6 nm. Furthermore, we characterized the structure of OA-coated UCNPs by XRD analysis (Figure 2A). The XRD results showed that the OA-coated UCNPs comprised a pure hexagonal phase and the positions and intensities of all the diffraction peaks agreed with data from the standard card for β-phase $NaLuF_4$ (Joint Committee on Powder Diffraction Standards card no 27-0726). No crystalline phase impurities were found in the diffraction pattern. Energy dispersive X-ray analysis showed that the main elemental components were Na, Lu, F, and Yb (Figure 2B). Due to the low content of doping Er ion (only 2 mol% Er among the rare-earth elements), the peak of the Er ion was generally not discerned. The results agreed with the actual components of co-doped $NaLuF_4$. Selected area electron diffraction and high-resolution TEM also demonstrated the highly crystalline nature of the synthesized nanoparticles (Figure 1A and C inset), and the results agreed well with the XRD data. The results agreed with the actual composition of the co-doped nanoparticles.

To allow the photothermal imaging, the UCNPs were then coated with a layer of PANPs. The preparation of the polyaniline-coated UCNPs (UCNPs-PANPs) is shown in Figure 3. The UCNPs-PANPs obtained were dispersed in ethanol. TEM images showed that the UCNPs-PANPs

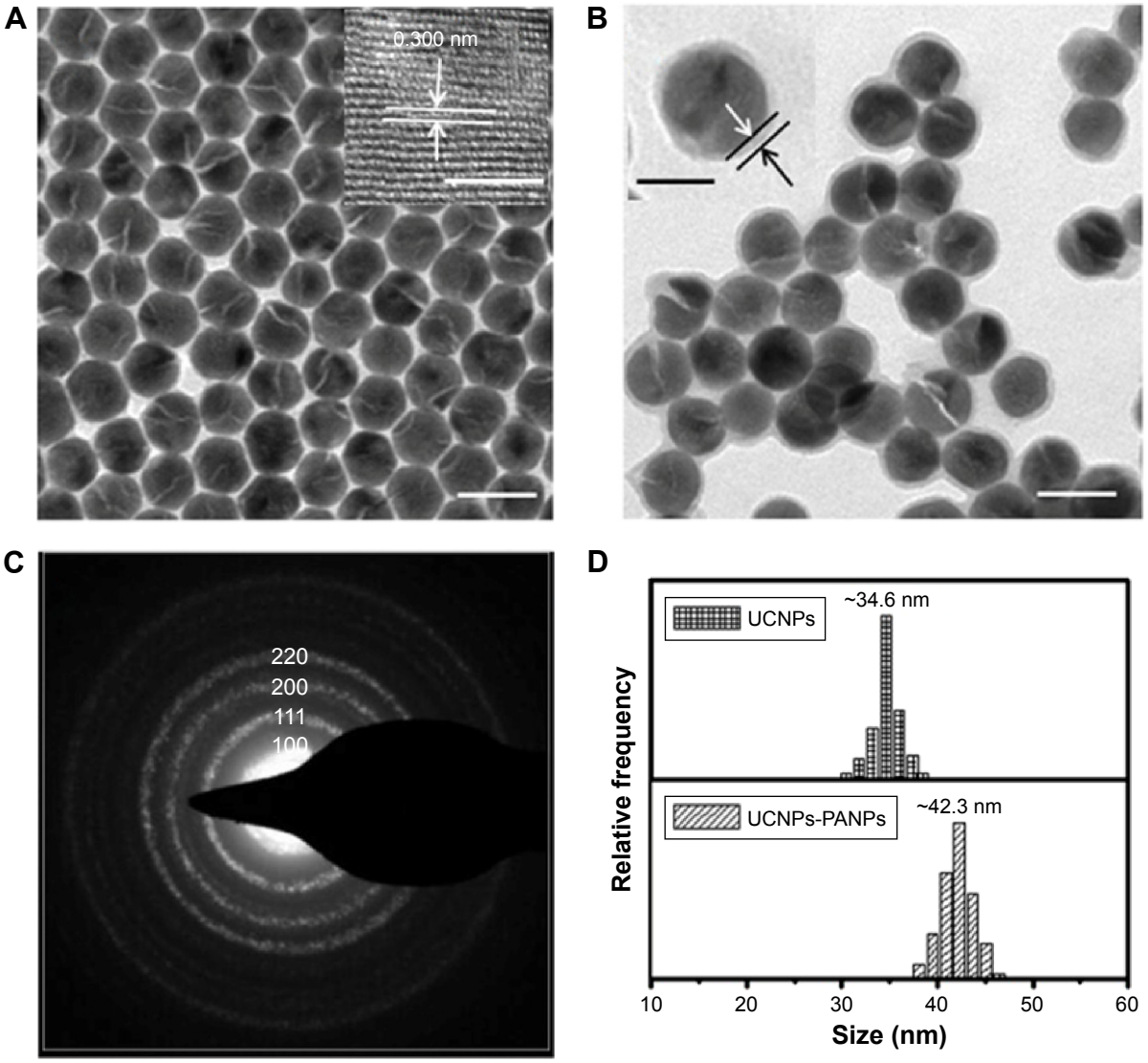

Figure 1 The morphology and size distribution of UCNPs-PANPs.
Notes: TEM image of UCNPs (**A**) and UCNPs-PANPs (**B**). Scale bar: 50 nm. Inset (**A**): an HR-TEM image of a UCNP. Arrows indicate the distance of the lattice. (Scale bar: 5 nm) and inset (**B**) a UCNP-PANP. Arrows indicates thickness of the shell (Scale bar: 30 nm). (**C**) SAED pattern of UCNPs. (**D**) The particle size distribution of UCNPs and UCNPs-PANPs. The average size of UCNPs and UCNPs-PANPs is ~34.6 nm and ~42.3 nm, respectively.
Abbreviations: HR-TEM, high-resolution transmission electron microscopy; SAED, selected area electron diffraction; UCNPs, upconversion nanoparticles; UCNPs-PANPs, polyaniline-coated UCNPs.

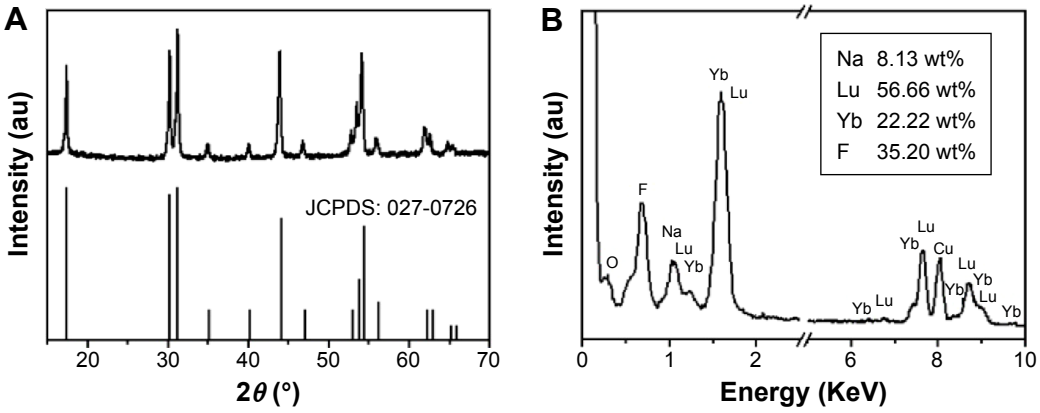

Figure 2 (*Continued*)

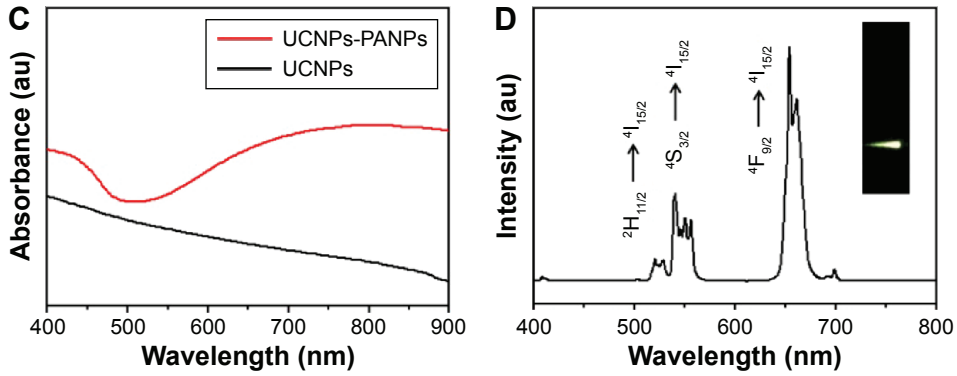

Figure 2 The crystalline phase, constituent, absorbance, and upconversion properties of UCNPs-PANPs.
Notes: XRD (**A**), the standard pattern of pure hexagonal $NaLuF_4$ (JCPDS card no 027-0726) and EDXA (**B**) pattern of UCNPs. The standard pattern of pure hexagonal $NaLuF_4$ (JCPDS card no 027-0726). (**C**) UV–vis–NIR absorbance spectra of UCNPs and UCNPs-PANPs. UCL spectrum (**D**) and photo (D inset) of UCNPs-PANPs solutions under excitation at continuous-wave 980 nm laser.
Abbreviations: UCL, upconversion luminescence; UCNPs, upconversion nanoparticles; UV–vis–NIR, ultraviolet–visible–near infrared; XRD, X-ray diffraction; UCNPs-PANPs, polyaniline-coated UCNPs; JCPDS, Joint Committee on Powder Diffraction Standards; EDXA, energy dispersive x-ray analysis.

measured ~42.3 nm and the thickness of the therapeutic shell was ~3.85 nm (Figure 1B and D). The absorption properties of the UCNPs-PANPs were studied by UV–vis–NIR spectroscopy (Figure 2C). Compared with the UCNPs, we found that the UCNPs-PANPs exhibited a strong NIR absorption band (600–900 nm), which was the characteristic of the PANPs.

UCL properties of UCNPs-PANPs

$NaLuF_4$ doped with Yb^{3+} and Er^{3+} is predicted to exhibit UCL properties. After excitation at 980 nm, we measured the emission spectra of the UCNPs-PANPs (1 mg mL^{-1}). The characteristic upconversion emission peaks of the UCNPs-PANPs in the visible region were located at 520 nm, 540 nm, and 654 nm, which corresponded to the Er^{3+} ion transitions of $^4H_{11/2} \rightarrow {}^4I_{15/2}$, $^4S_{3/2} \rightarrow {}^4I_{15/2}$, and $^4F_{9/2} \rightarrow {}^4I_{15/2}$, respectively (Figure 2D). The green emission at 520–560 nm and the red emission at 640–680 nm led to the emission of visible yellow light in water (Figure 2D inset). Moreover, the intrinsic emission band of UCNPs-PANPs was very narrow (full width at half-maximum is 12 nm). These results indicate that UCNPs-PANPs can be used as a suitable upconversion matrix material for UCL imaging of cancer cells. Based on previous reports of similar nanoparticles,[31,32] UCNPs-PANPs are expected to completely eliminate autofluorescence from biotissues during bioimaging, and they can be successfully

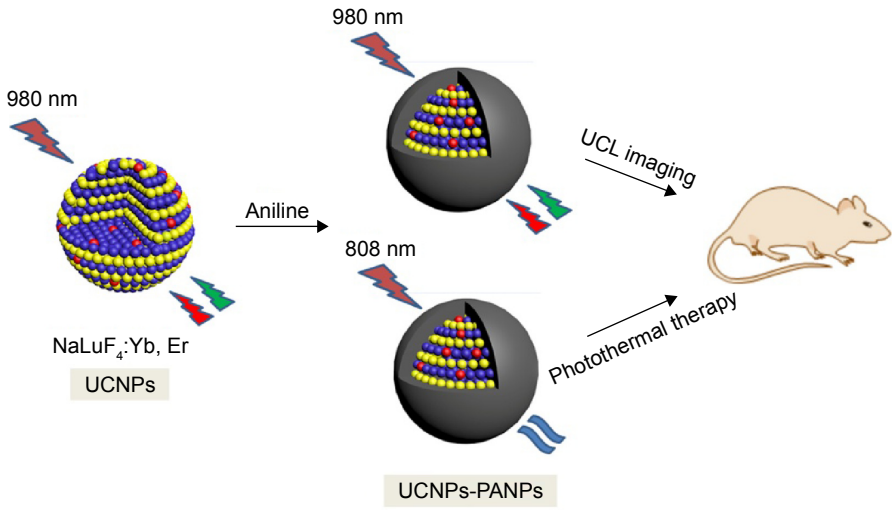

Figure 3 Schematic illustration of synthesis of $NaLuF_4$:Yb, Er (UCNPs), and polyaniline-coated UCNPs (UCNPs-PANPs) and their applications in UCL imaging and photothermal therapy.
Notes: Upon 980 nm excitation, both UCNPs and UCNPs-PANPs emitted green and red emissions. Upon 808 nm, UCNPs-PANPs could convert laser light into heat.
Abbreviations: UCL, upconversion luminescence; UCNPs, upconversion nanoparticles; UCNPs-PANPs, polyaniline-coated UCNPs.

applied in the bioimaging of various biological samples, including living cells and small animals.

Photothermal conversion efficiency of UCNPs-PANPs

After collecting the thermal radiation signal generated by the PTT coupling agents, photothermal images were recorded using photothermal imaging equipment (Figure 4A). Photothermal imaging was investigated by monitoring UCNP-PANP solutions (1 mg mL^{-1}) irradiated by an 808 nm laser at various power densities (0.50 W cm^{-2}, 0.85W cm^{-2}, and 1.20 W cm^{-2}; Figure 4B). The thermal signals of the UCNPs-PANPs increased gradually within 5 minutes and the temperature increased from room temperature (30.0°C) to 42.0°C at 0.50 W cm^{-2}, 50.0°C at 0.85 W cm^{-2}, and 60.0°C at 1.20 W cm^{-2} (Figure 4C). These results indicate that the UCNP-PANP samples could absorb and convert light into a substantial amount of heat energy. Moreover, we measured the photothermal conversion efficiency (η) of the UCNPs-PANPs. According to the equations, the η value for the UCNPs-PANPs was determined as 47.8% (Figure 4D and E), which is quite similar to that of previously reported PANPs.[30] The photostability of the UCNP-PANP solution was also studied using a photothermal imaging system. The temperatures of the UCNPs-PANPs remained at the same level after five cycles of NIR laser-induced heating (808 nm laser at 1.20 W cm^{-2}, 2 minutes laser irradiation for each cycle; Figure 4F). The photostability of the UCNPs-PANPs was much better than that of Au nanorods, for which the absorbance peak decreased under laser irradiation after a long period of laser exposure. Our results indicate that these UCNPs-PANPs with high photothermal conversion efficiency and photostability could be used as a photothermal agent.

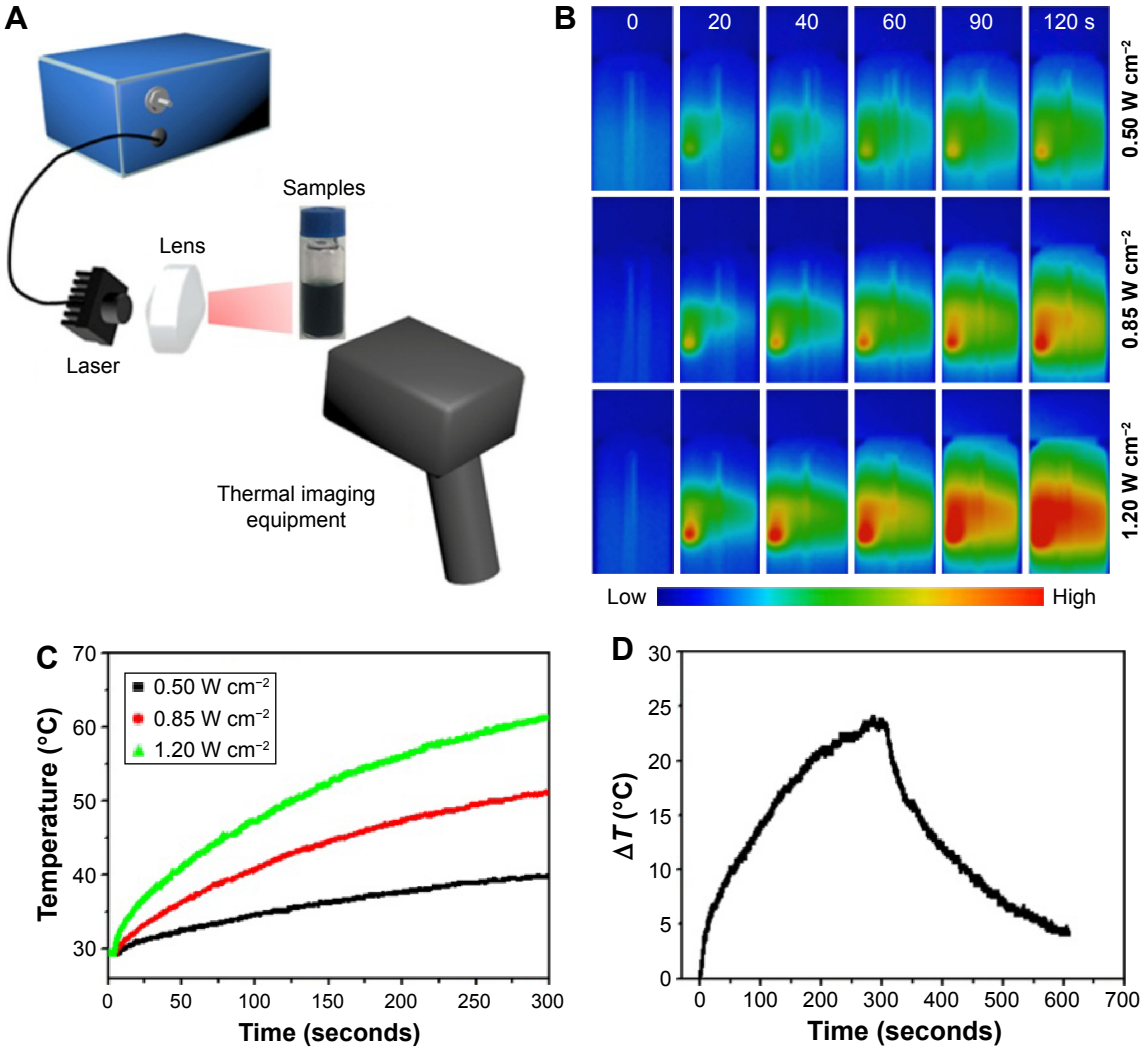

Figure 4 (*Continued*)

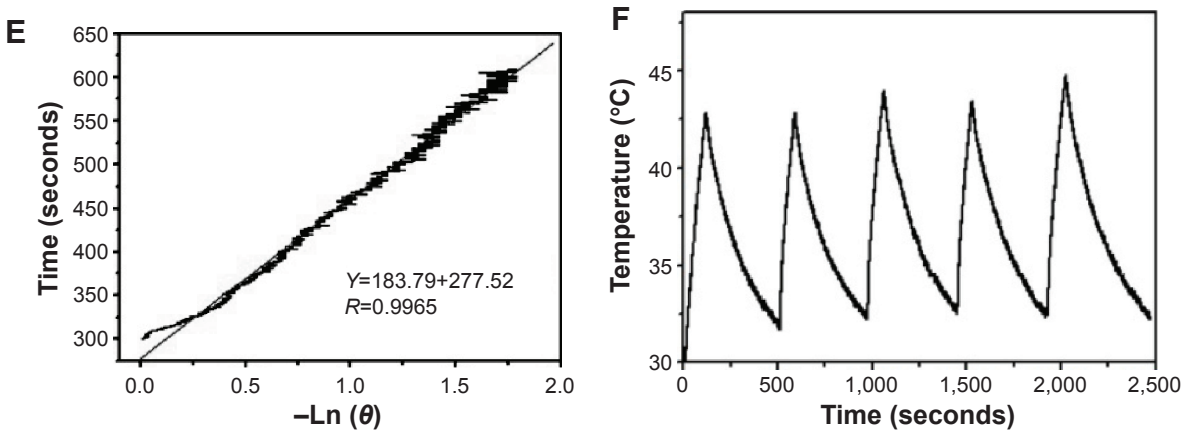

Figure 4 Photothermal conversion properties of UCNPs-PANPs.
Notes: (**A**) Schematic illustration of the photothermal system. Photothermal images (**B**) and heating curves (**C**) of UCNPs-PANPs (1 mg mL^{-1}) under 808 nm laser irradiation at the power density of 0.50 W cm^{-2}, 0.85 W cm^{-2}, and 1.20 W cm^{-2}. (**D**) Heating curves of UCNPs-PANPs (200 μg mL^{-1}) under 808 nm NIR laser irradiation at the power density of 0.80 W cm^{-2}. The NIR laser irradiation was stopped after 5 minutes. (**E**) Linear time data vs –ln θ obtained from the cooling period of (**D**). (**F**) Temperature variations of UCNPs-PANPs (200 μg mL^{-1}) under the continuous irradiations of 808 nm laser (1.20 W cm^{-2}) for five cycles.
Abbreviations: NIR, near infrared; UCNPs, upconversion nanoparticles; UCNPs-PANPs, polyaniline-coated UCNPs.

Cytotoxicity of UCNPs-PANPs

For bioapplications, UCNPs-PANPs were further capped with F127 according to a previous study.[30] Zeta potential and hydrodynamic diameter were also measured. The zeta potential of the UCNPs-PANPs was ~0 and dynamic light scattering measurements showed that the effective hydrodynamic diameter of the UCNPs-PANPs was ~120 nm (Figure S1). The cytotoxicity of UCNPs-PANPs needs to be investigated before their use as a potential PTT agent. Thus, the UCNPs-PANPs were delivered over a wide range of dosages (0–800 μg mL^{-1} in our experiment) to cancer cells, and their reduced activity in the MTT assay was employed to test their cytotoxicity (Figure 5A). Cell viability of 80% was observed with the UCNPs-PANPs even at a high-dose concentration of 800 μg mL^{-1} after treatment for 48 hours, thereby indicating that the UCNPs-PANPs exhibited relatively low cytotoxicity. Serum biochemistry assays were also performed to investigate cytotoxicity, where hepatic and kidney indicators (TBIL, ALT, AST, TP, ALB, and CRE) were measured (Figure 5B). The indicators of liver and kidney functions were similar to those in the blank groups. For histological studies, mice were injected intravenously with the UCNPs-PANPs (100 μL, 2 mg mL^{-1}), and the main organs of interest (heart, liver, spleen, lung, and kidney) were harvested at 30 days post injection. Mice that received no injection were used for comparison (control). H&E staining detected no evidence of adverse effects caused by the UCNPs-PANPs (Figure 5C). These results suggest that the UCNPs-PANPs had no cytotoxic effects on cancer cells and the animal model at the dose tested dose in our study.

Photothermal imaging in vivo

Based on their efficient upconversion luminescent properties, high photothermal conversion efficiency, and low cytotoxicity, the UCNPs-PANPs were tested to assess their possible use as a PTT coupling agent based on further in vitro and in vivo tests. Cells internalized UCNPs-PANPs (100 μg mL^{-1}), and they were exposed to an 808 nm laser (0.5 W cm^{-2}) for 15 minutes. After various combinations of treatments with UCNPs-PANPs and NIR lasers, fluorescent staining was used to assess the cells with propidium iodide (a dye was used for identifying dead cells in a population). After detecting the emissions at 600−640 nm, an intense fluorescent signal was detected from the cancer cells (Figure 6A right). Merging of the fluorescent image and bright-field image showed that the fluorescence originated from the intracellular region (Figure 6A left). We found that cancer cells treated with UCNPs-PANPs and exposed to an NIR laser exhibited substantial cellular death, and the cytotoxicity of the UCNPs-PANPs against cancer cells was also irradiation time dependent (Figure S2). Thus, UCNPs-PANPs may be considered as extremely promising candidates for mediating the photothermal destruction of tumors in vivo. A PBS solution of UCNPs-PANPs (50 μL, 1 mg mL^{-1}) was injected intratumorally into nude mice, which were then irradiated by an 808 nm laser at a power density of 0.5 W cm^{-2}. Photothermal imaging was used to record the temperature changes, which showed that the surface temperature of the tumor increased rapidly from 31.2°C to 45.8°C within 60 seconds (Figure 6B). These results indicate that the enhanced temperature of the tumor was sufficiently high to kill the cancer cells.

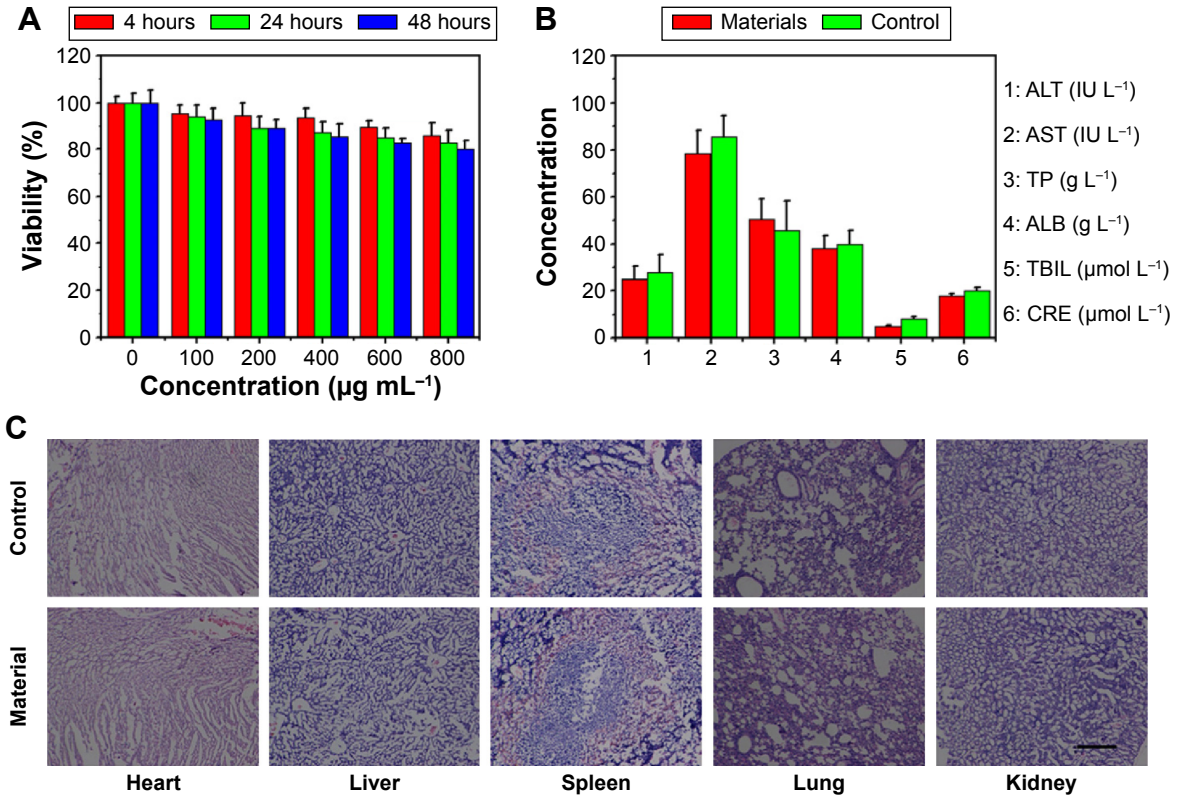

Figure 5 Cytotoxicity of UCNPs-PANPs.

Notes: (**A**) In vitro cell viability of cancer cells incubated with UCNPs-PANPs with different concentrations (0 μg mL^{-1}, 100 μg mL^{-1}, 200 μg mL^{-1}, 400 μg mL^{-1}, 600 μg mL^{-1}, and 800 μg mL^{-1}) for 4 hours, 24 hours, and 48 hours at 37°C. (**B**) Serum biochemistry results obtained from mice injected with UCNPs-PANPs (100 μL, 2 mg mL^{-1}) 30 days post injection (material) and mice receiving no injection (control). (**C**) H&E-stained tissue sections from mice injected with UCNPs-PANPs 30 days post injection (materials) and mice receiving no injection (control). Tissues were harvested from kidney, lung, spleen, liver, and heart. Scale bar: 100 μm.

Abbreviations: ALB, albumin; ALT, alanine aminotransferase; AST, aspartate amino transferase; CRE, creatinine; H&E, hematoxylin and eosin; TBIL, total bilirubin; TP, total protein; UCNPs, upconversion nanoparticles; UCNPs-PANPs, polyaniline-coated UCNPs.

PTT in vivo

We also studied UCNPs-PANPs-induced photothermal cancer therapy in vivo using four groups of U87MG tumor-bearing mice. In the test group, mice were injected intratumorally with a PBS solution of UCNPs-PANPs (50 μL, 1 mg mL^{-1}) and exposed to an 808 nm laser (material + laser, n=3). For comparison, mice that were not injected with UCNPs-PANPs (laser, *n*=3) and not exposed to the 808 nm laser (material, n=3) were used as the control groups. The blank group comprised mice that received no injection of UCNPs-PANPs and no exposure to the 808 nm laser (blank, n=3). After irradiation at 0.5 W cm^{-2} for 10 minutes, the tumors

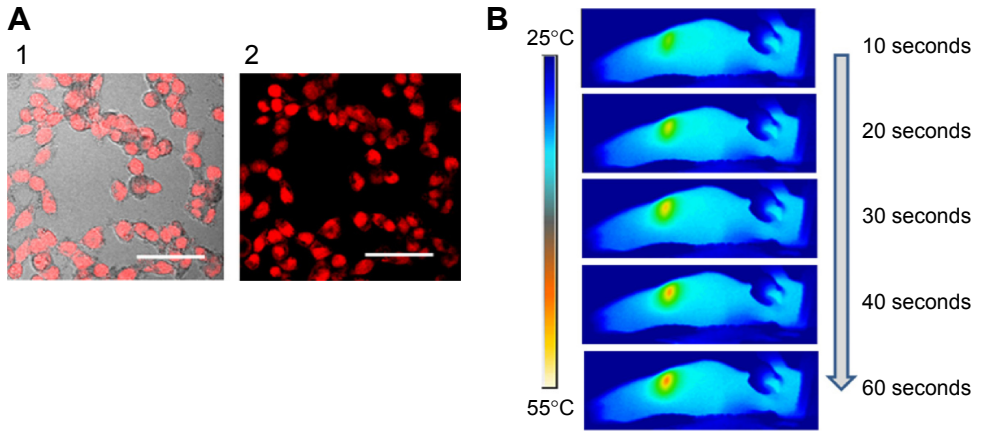

Figure 6 (*Continued*)

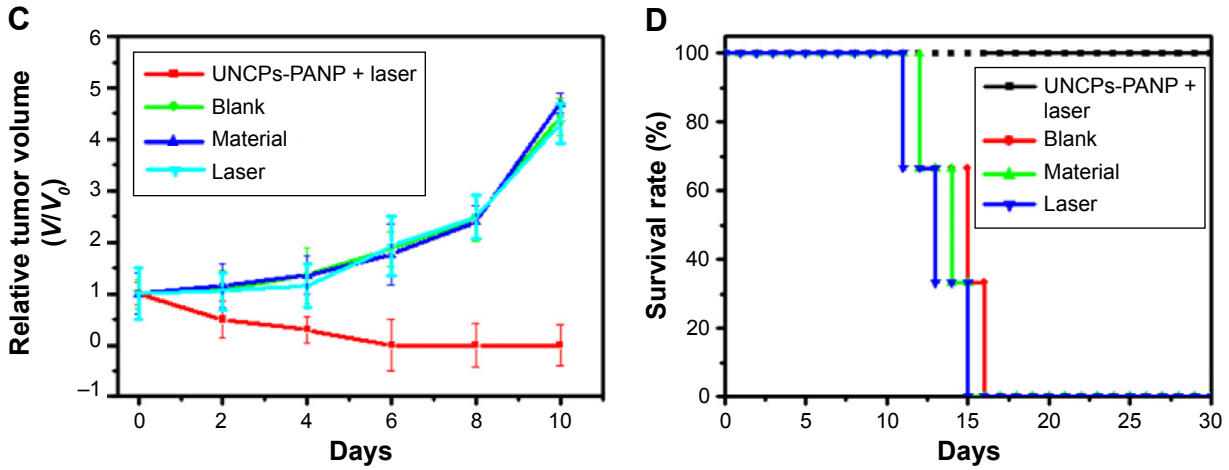

Figure 6 Photothermal imaging and therapy of UCNPs-PANPs.
Notes: (**A**) Cancer cells were first incubated with UCNPs-PANPs samples (100 μg mL^{-1}) for 4 hours and irradiated by 808 nm laser (0.5 W cm^{-2}) for 15 minutes. Cells were then stained with PI for 10 minutes (2). The overlay of fluorescence image and bright-field image (1). (**B**) Photothermal images of nude mouse injected with UCNPs-PANPs (50 μL, 1 mg mL^{-1}) exposed to the 808 nm laser at the power densities of 0.5 W cm^{-2} recorded within 60 seconds. Tumor growth rates (**C**) and survival curves (**D**) of experiment group (UCNPs-PANPs + laser), materials group (UCNPs-PANPs), laser group (laser), and blank group (blank).
Abbreviations: PI, propidium iodide; UCNPs, upconversion nanoparticles; UCNPs-PANPs, polyaniline-coated UCNPs.

began to shrink in the test group. On day 6, the tumors were eliminated completely, and only black scars remained at the original tumor sites. Tumor regrowth was not observed from day 6 to day 10. By contrast, the tumors in the control and the blank groups exhibited rapid growth throughout the 10-day period. The relative tumor volume (V/V_0) was used to quantitatively measure the size of the tumor. The V/V_0 for the test group had decreased to ~0 on day 6, and the V/V_0 remained at 0 from day 6 to day 10. By contrast, the V/V_0 in the control and blank groups increased from 1 to 5 during the 10-day treatment period (Figure 6C). These results demonstrate that NIR laser irradiation or UCNPs-PANPs injection alone did not affect tumor development. The life spans of the mice were also recorded after treatment. The mice in the test group survived for >1 month without tumor regeneration and death. (Figure 6D). However, the mice in the control and blank groups were humanely euthanized on day 14 when the growing tumors showed signs of affecting their normal lives. Our results demonstrate the excellent efficacy of the UCNPs-PANPs for use of in vivo photothermal cancer therapy.

Conclusion

In this study, uniform UCNPs measuring ~34.6 nm were synthesized by a solvothermal method and further coated with a shell of polyaniline (thickness =~3.85 nm). The UCNPs-PANPs exhibited several potential advantages: efficient UCL (520–560 nm and 640–680 nm), high photothermal conversion efficiency (47.8%), high photostability, and low cytotoxicity to living cells and mammals. Finally, the UCNPs-PANPs were applied successfully to imaging-guided PTT in vitro and in vivo. The development of UCNPs-PANPs may provide a platform technology for the next generation of imaging-guided therapy in tumor-bearing mice.

Acknowledgment

The authors thank the National Natural Science Foundation of China (23173268) for funding.

Disclosure

The authors report no conflicts of interest in this work.

References

1. Cheng L, Wang C, Feng LZ, Yang K, Liu Z. Functional nanomaterials for phototherapies of cancer. *Chem Rev*. 2014;114(21):10869–10939.
2. Jain PK, Huang X, El-Sayed IH, El-Sayed MA. Noble metals on the nanoscale: optical and photothermal properties and some applications in imaging, sensing, biology, and medicine. *Acc Chem Res*. 2008;41(12):1578–1586.
3. Zhou ZG, Kong B, Yu C, et al. Tungsten oxide nanorods: an efficient nanoplatform for tumor CT imaging and photothermal therapy. *Sci Rep*. 2014;4:3653.
4. Yin WY, Yan L, Yu J, et al. High-throughput synthesis of single-layer MoS_2 nanosheets as a near-infrared photothermal-triggered drug delivery for effective cancer therapy. *ACS Nano*. 2014;8(7):6922–6933.
5. Wang SG, Li K, Chen Y, et al. Biocompatible pegylated MoS_2 nanosheets: controllable bottom-up synthesis and highly efficient photothermal regression of tumor. *Biomaterials*. 2015;39(0):206–217.
6. Huang XQ, Tang SH, Yang J, Tan YM, Zheng NF. Etching growth under surface confinement: an effective strategy to prepare mesocrystalline Pd nanocorolla. *J Am Chem Soc*. 2011;133(40):15946–15949.
7. Averitt RD, Sarkar D, Halas NJ. Plasmon resonance shifts of Au-coated Au_2S nanoshells: insight into multicomponent nanoparticle growth. *Phys Rev Lett*. 1997;78(22):4217–4220.

8. Hirsch LR, Stafford RJ, Bankson JA, et al. Nanoshell-mediated near-infrared thermal therapy of tumors under magnetic resonance guidance. *Proc Natl Acad Sci U S A*. 2003;100(23):13549–13554.
9. Loo C, Lowery A, Halas N, West J, Drezek R. Immunotargeted nanoshells for integrated cancer imaging and therapy. *Nano Lett*. 2005;5(4):709–711.
10. Song GS, Wang Q, Wang Y, et al. A low-toxic multifunctional nanoplatform based on Cu_9S_5@$mSiO_2$ core-shell nanocomposites: combining photothermal- and chemotherapies with infrared thermal imaging for cancer treatment. *Adv Funct Mater*. 2013;23(35):4281–4292.
11. Tian QW, Tang MH, Sun YG, et al. Hydrophilic flower-like CuS superstructures as an efficient 980 nm laser-driven photothermal agent for ablation of cancer cells. *Adv Mater*. 2011;23(31):3542–3547.
12. Yang D, Yang GX, Wang XM, et al. Y_2O_3:Yb,Er@$mSiO_2$-Cu_xS double-shelled hollow spheres for enhanced chemo-/photothermal anti-cancer therapy and dual-modal imaging. *Nanoscale*. 2015;7(28):12180–12191.
13. Hong GS, Diao S, Antaris AL, Dai HJ. Carbon nanomaterials for biological imaging and nanomedicinal therapy. *Chem Rev*. 2015;115(19):10816–10906.
14. Xu LG, Cheng L, Wang C, Peng R, Liu Z. Conjugated polymers for photothermal therapy of cancer. *Polym Chem*. 2014;5(5):1573–1580.
15. Chen M, Fang XL, Tang SH, Zheng NF. Polypyrrole nanoparticles for high-performance *in vivo* near-infrared photothermal cancer therapy. *Chem Commun*. 2012;48(71):8934–8936.
16. Yang K, Xu H, Cheng L, Sun C, Wang J, Liu Z. *In vitro* and *in vivo* near-infrared photothermal therapy of cancer using polypyrrole organic nanoparticles. *Adv Mater*. 2012;24(41):5586–5592.
17. Zha ZB, Yue XL, Ren QS, Dai ZF. Uniform polypyrrole nanoparticles with high photothermal conversion efficiency for photothermal ablation of cancer cells. *Adv Mater*. 2012;25(5):777–782.
18. Tao Y, Ju EG, Ren JS, Qu XG. Polypyrrole nanoparticles as promising enzyme mimics for sensitive hydrogen peroxide detection. *Chem Commun*. 2014;50(23):3030–3032.
19. Li LY, Liu YX, Hao PL, et al. PEDOT nanocomposites mediated dual-modal photodynamic and photothermal targeted sterilization in both NIR I and II window. *Biomaterials*. 2015;41(0):132–140.
20. Xu H, Pang XC, He YJ, et al. An unconventional route to monodisperse and intimately contacted semiconducting organic–inorganic nanocomposites. *Angew Chem Int Ed*. 2015;54(15):4636–4640.
21. Lin LS, Cong ZX, Cao JB, et al. Multifunctional Fe_3O_4@polydopamine core–shell nanocomposites for intracellular mRNA detection and imaging-guided photothermal therapy. *ACS Nano*. 2014;8(4):3876–3883.
22. Ju EG, Dong K, Liu Z, Pu F, Ren JS, Qu XG. Tumor microenvironment activated photothermal strategy for precisely controlled ablation of solid tumors upon NIR irradiation. *Adv Funct Mater*. 2015;25(10):1574–1580.
23. Jiang NN, Ruan QF, Qin F, Wang JF, Lin HQ. Switching plasmon coupling through the formation of dimers from polyaniline-coated gold nanospheres. *Nanoscale*. 2015;7(29):12516–12526.
24. Lee T, Bang D, Park Y, et al. Gadolinium-enriched polyaniline particles (GPAPs) for simultaneous diagnostic imaging and localized photothermal therapy of epithelial cancer. *Adv Healthc Mater*. 2014;3(9):1408–1414.
25. Hsiao CW, Chen HL, Liao ZX, et al. Effective photothermal killing of pathogenic bacteria by using spatially tunable colloidal gels with nanolocalized heating sources. *Adv Funct Mater*. 2014;25(5):721–728.
26. Abel SB, Molina MA, Rivarola CR, Kogan MJ, Barbero CA. Smart polyaniline nanoparticles with thermal and photothermal sensitivity. *Nanotechnology*. 2014;25(49):495602.
27. Hsiao CW, Chuang EY, Chen HL, et al. Photothermal tumor ablation in mice with repeated therapy sessions using NIR-absorbing micellar hydrogels formed *in situ*. *Biomaterials*. 2015;56(0):26–35.
28. Hong Y, Hwang S, Heo D, et al. A magnetic polyaniline nanohybrid for MR imaging and redox sensing of cancer cells. *Nanoscale*. 2015;7(5):1661–1666.
29. Yang J, Choi J, Bang D, et al. Convertible organic nanoparticles for near-infrared photothermal ablation of cancer cells. *Angew Chem Int Ed*. 2011;50(2):441–444.
30. Zhou J, Lu ZG, Zhu XJ, et al. NIR photothermal therapy using polyaniline nanoparticles. *Biomaterials*. 2013;34(37):9584–9592.
31. Zhou J, Liu Q, Feng W, Sun Y, Li FY. Upconversion luminescent materials: advances and applications. *Chem Rev*. 2015;115(1):395–465.
32. Zhou J, Liu Z, Li FY. Upconversion nanophosphors for small-animal imaging. *Chem Soc Rev*. 2012;41(3):1323–1349.
33. Dong H, Du SR, Zheng XY, et al. Lanthanide nanoparticles: from design toward bioimaging and therapy. *Chem Rev*. 2015;115(19):10725–10815.
34. Li XM, Zhang F, Zhao DY. Lab on upconversion nanoparticles: optical properties and applications engineering *via* designed nanostructure. *Chem Soc Rev*. 2015;44(6):1346–1378.
35. Liu X, Yan CH, Capobianco JA. Photon upconversion nanomaterials. *Chem Soc Rev*. 2015;44(6):1299–1301.
36. Liu XW, Deng RR, Zhang YH, et al. Probing the nature of upconversion nanocrystals: instrumentation matters. *Chem Soc Rev*. 2015;44(6):1479–1508.
37. Idris NM, Jayakumar MKG, Bansal A, Zhang Y. Upconversion nanoparticles as versatile light nanotransducers for photoactivation applications. *Chem Soc Rev*. 2015;44(6):1449–1478.
38. Chen G, Agren H, Ohulchanskyy TY, Prasad PN. Light upconverting core-shell nanostructures: nanophotonic control for emerging applications. *Chem Soc Rev*. 2015;44(6):1680–1713.
39. Hou ZY, Zhang YX, Deng KR, et al. UV-emitting upconversion-based TiO_2 photosensitizing nanoplatform: near-infrared light mediated *in vivo* photodynamic therapy *via* mitochondria-involved apoptosis pathway. *ACS Nano*. 2015;9(3):2584–2599.
40. Cheng L, Yang K, Li YG, et al. Multifunctional nanoparticles for upconversion luminescence/MR multimodal imaging and magnetically targeted photothermal therapy. *Biomaterials*. 2012;33(7):2215–2222.
41. Ni DL, Bu WB, Zhang SJ, et al. Single Ho^{3+}-doped upconversion nanoparticles for high-performance T_2-weighted brain tumor diagnosis and MR/UCL/CT multimodal imaging. *Adv Funct Mater*. 2014;24(42):6613–6620.
42. Zhang YL, Liu XH, Lang YB, et al. Synthesis of ultra-small $BaLuF_5$:Yb^{3+},Er^{3+}@$BaLuF_5$:Yb^{3+} active-core-active-shell nanoparticles with enhanced up-conversion and down-conversion luminescence by a layer-by-layer strategy. *J Mater Chem C*. 2015;3(9):2045–2053.
43. Zhou L, Li ZH, Ju EG, Liu Z, Ren JS, Qu XG. Aptamer-directed synthesis of multifunctional lanthanide-doped porous nanoprobes for targeted imaging and drug delivery. *Small*. 2013;9(24):4262–4268.
44. Song HW, Chen BT, Dong B, et al. Amphiphilic silane modified $NaYF_4$:Yb,Er loaded with $Eu(TTA)_3(TPPO)_2$ nanoparticles and the multi-functions: dual mode temperature sensing and cell imaging. *Nanoscale*. 2013;5(18):8541–8549.
45. Zhou J, Lu ZG, Shan GG, Wang SH, Liao Y. Gadolinium complex and phosphorescent probe-modified $NaDyF_4$ nanorods for T_1- and T_2-weighted MRI/CT/phosphorescence multimodality imaging. *Biomaterials*. 2014;35(1):368–377.
46. Jalil RA, Zhang Y. Biocompatibility of silica coated $NaYF_4$ upconversion fluorescent nanocrystals. *Biomaterials*. 2008;29(30):4122–4128.
47. Dong AG, Ye XC, Chen J, et al. A generalized ligand-exchange strategy enabling sequential surface functionalization of colloidal nanocrystals. *J Am Chem Soc*. 2010;133(4):998–1006.
48. Liu Y, Ai K, Liu J, Deng M, He Y, Lu L. Dopamine-melanin colloidal nanospheres: an efficient near-infrared photothermal therapeutic agent for *in vivo* cancer therapy. *Adv Mater*. 2013;25(9):1353–1359.

Supplementary materials

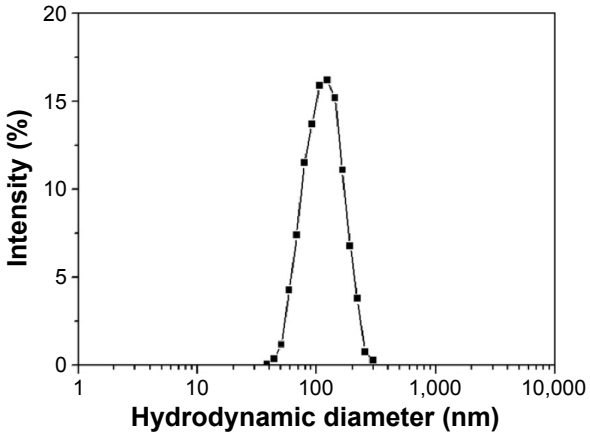

Figure S1 The hydrodynamic diameter distribution of UCNP-PANPs by DLS measurement.
Abbreviations: DLS, dynamic light scattering; UCNPs, upconversion nanoparticles; UCNPs-PANPs, polyaniline-coated UCNPs.

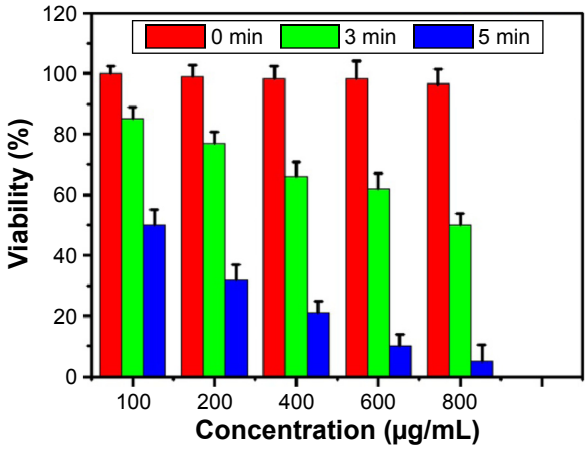

Figure S2 In vitro cell viability of cancer cells after treatment with different concentrations of UCNP-PANPs and different NIR laser irradiation time.
Abbreviations: NIR, near infrared; UCNPs, upconversion nanoparticles; UCNPs-PANPs, polyaniline-coated UCNPs.